# Extracting coupling and loss coefficients from a ring resonator

**W. R. McKinnon, D.-X. Xu, C. Storey, E. Post, A. Densmore, A. Delâge, P. Waldron, J. H. Schmid, and S. Janz**

*Institute for Microstructural Sciences, National Research Council of Canada, 1200 Montreal Road, Ottawa, Ontario, Canada, K1A 0R6*

*ross.mckinnon@nrc-cnrc.gc.ca*

**Abstract:** A method is developed for extracting the coupling and loss coefficients of ring resonators from the peak widths, depths, and spacings of the resonances of a single resonator. Although the formulas used do not distinguish which coefficient is coupling and which is loss, it is shown how these coefficients can be disentangled based on how they vary with wavelength or device parameters.

**OCIS codes:** (130.3120) Integrated optics devices; (220.0220) Optical design and fabrication; (230.5750) Resonators; (130.6010) Sensors; (120.0120) Instrumentation, measurement, and metrology.

## References and links

1. D. Po, S.F. Preble, and M. Lipson, "All-optical compact silicon comb switch," Opt. Express **15**, 9600-9605 (2007)
2. B. E. Little, S. T. Chu, H. A. Haus, J. Foresi and J.-P. Laine, "Microring resonator channel dropping filters," J. Lightwave Technol. **15**, 998-1005 (1997).
3. D.-X. Xu, A. Densmore, A. Delâge, P. Waldron, R. McKinnon, S. Janz, J. Lapointe, G. Lopinski, T. Mischki, E. Post, P. Cheben, and J. H. Schmid, "Folded cavity SOI microring sensors for high sensitivity and real time measurement of biomolecular binding," Opt. Express **16**, 15137–15148 (2008).
4. D.G. Rabus, *Integrated Ring Resonators: the Compedium* (Springer-Verlag, Berlin 2007).
5. J. E. Heebner, V. Wong, A. Schweinsberg, R. W. Boyd, and D. J. Jackson, "Optical Transmission Characteristics of Fiber Ring Resonators," IEEE J. Quantum Electron. **40** 726-370 (2004).
6. F. Xia, L. Sekaric, and Y. A. Vlasov, "Mode conversion losses in silicon-on-insulator photonic wire based racetrack insulators," Opt. Express **14**, 3872-3886 (2006).
7. J. Scheuer, " Fabrication and Characterization of Low-Loss Polymeric Waveguides and Micro-Resonators," in *Integrated Photonics and Nanophotonics Research and Applications*, OSA Technical Digest (CD) (Optical Society of America, 2007), paper ITuA3.
8. J. Niehusmann, A. Vorckel, P. H. Bolivar, T. Wahlbrink, W. Henschel, and H. Kurz, "Ultrahigh-quality-factor silicon-on-insulator microring resonator," Opt. Lett. **29**, 2861-2863 (2004).
9. A. Yariv, "Universal relations for coupling of optical power between microresonators and dielectric waveguides," Electron. Lett. 36, 321-322 (2000).
10. A. Delâge, D.-X. Xu, W. R. McKinnon, E. Post, P. Waldron, J. Lapointe, C. Storey, A. Densmore, S. Janz, B. Lamontagne, P. Cheben and J. H. Schmid, "Wavelength Dependent Model of a Ring Resonator Sensor Excited by a Directional Coupler," J. Lightwave Tech. **27**, 1172-80 (2009).
11. G. Gupta, Y.-H. Kuo, H. Tazawa, W. Steier, A. Stapleton, and J. O'Brien, "Analysis and Demonstration of Coupling Control in Polymer Microring Resonators Using Photobleaching," Appl. Opt. (to be published).
12. L. F. Stokes, M. Chodorow, and H. J. Shaw, "All-single-mode fiber resonator," Opt. Lett. **7** 288-290 (1982).
13. R. Loudon, *The quantum theory of light*, 3rd ed (Oxford University Press, Oxford 2000).
14. D.-X. Xu, S. Janz, and P. Cheben, "Design of Polarization-Insensitive Ring Resonators in Silicon-on-Insulator Using MMI Couplers and Cladding Stress Engineering," IEEE Photon. Tech. Lett. **18**, 343-345 (2006).
15. A. Densmore and D.-X. Xu, unpublished results.

#115559 - $15.00 USD Received 10 Aug 2009; revised 21 Sep 2009; accepted 27 Sep 2009; published 6 Oct 2009

## 1. Introduction

Ring resonators are an important optical component in modulators and switches [1], filters [2], and sensors [3]. Their properties have been extensively studied and are treated in two recent monographs [4], [5].

The performance of a ring resonator is determined by two coefficients: the self-coupling coefficient $t$, which specifies the fraction of the amplitude transmitted on each pass of light through the coupler; and the loss coefficient $\alpha$, which specifies the fraction of the amplitude transmitted per pass around the ring. In optimizing the design of a ring resonator, it is important to extract and distinguish these coefficients, as they are governed by different factors in design and fabrication. So far, most determinations of $\alpha$ and $t$ from experimental measurements have been based on a single resonance [6] - [8], or on special structures that are more complicated than a single ring [8]. For the transmission past a simple ring resonator with a single coupler, $\alpha$ and $t$ enter the expression for the lineshape symmetrically [9], so that the same resonance profile is produced if the two coefficients are interchanged. As a result, it cannot be determined which extracted coefficient is $\alpha$ and which is $t$ from the analysis of a single resonance [8].

More complicated structures have been proposed to disentangle the two coefficients [6]. This involves comparing different devices, and assuming that the devices have identical couplers. Here we show that an alternative approach is to examine how the coefficients vary with wavelength or with device dimensions. In a ring with a directional coupler (DC), $t$ varies approximately sinusoidally with wavelength [10]. On the other hand, $\alpha$ is not expected to depend this strongly on $\lambda$ when the bending losses are small. (For the devices in silicon-on-insulator (SOI) considered here, the bending losses should be small for radii larger than 5 $\mu$m.) Alternatively, if devices with different sizes of couplers or optical path length are available, the coefficients can be identified by how they vary between devices. Resonators with different path lengths but similar couplers should have similar $t$ but different $\alpha$, for example.

Through analyzing SOI photonic wire ring resonators with a range of design parameters, we demonstrate how to extract and distinguish $\alpha$ and $t$ through the dependence on $\lambda$. We give examples where this method works well in a single device when the cross-coupling is strong enough, and we show how to extend the method to the case of weaker cross-coupling by comparing devices with different radii or coupler geometry.

Our approach does not involve the measurement of phase. If the phase is determined, it is possible to distinguish whether the ring is undercoupled ($t > \alpha$) or overcoupled ($t < \alpha$) [5], [11], and thus disentangle $t$ and $\alpha$. Such measurements require additional equipment such as a network analyzer [11], or more complex devices such as rings coupled to Mach-Zehnder interferometers [5]. Our approach requires only intensity measurements using a variable wavelength source on isolated resonators.

In the following, Section 2 reviews the equations of the resonances of a ring resonator, and gives expressions for the self-coupling and loss coefficients in terms of the finesse and the depth of the resonances. Section 3 discusses the measurements and data analysis. Section 4 considers several devices that illustrate the concepts.

## 2. Theory

We begin by reviewing the theory of a simple ring resonator, to clarify the meaning of the coefficients. Figure 1 shows schematically a ring resonator with a single directional coupler (DC), and gives the notation used. For the coupler in Fig. 1b, the fields $b$ and $b'$ at the outputs are related to the fields $a$ and $a'$ at the inputs by self-coupling coefficients $t_c$ and $t_c'$, and the cross-coupling coefficients $\kappa_c$ and $\kappa_c'$, according to Eqs. (1) and (2):

$$b = t_c a + \kappa_c' a'; \quad (1)$$

#115559 - $15.00 USD Received 10 Aug 2009; revised 21 Sep 2009; accepted 27 Sep 2009; published 6 Oct 2009

$$b' = t_c' a' + \kappa_c a. \tag{2}$$

If the output $b'$ is coupled back to the input $a'$ as in Fig. 1a, through a coefficient $t_r'$, then $a'$ is given by Eq. (3):

$$a' = t_r' b'. \tag{3}$$

Substituting Eq. (3) into Eq. (2) gives Eq. (4):

$$b = \frac{t_c - (t_c t_c' - \kappa_c \kappa_c')t_r'}{} a. \tag{4}$$

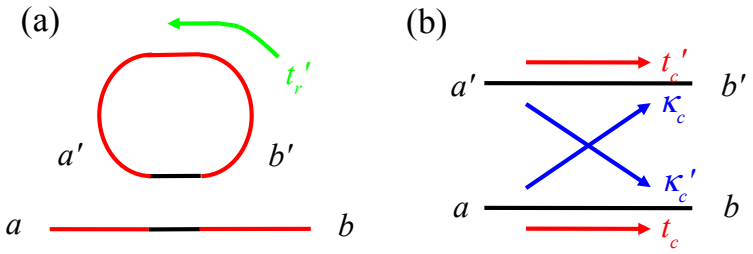


Fig. 1. Ring resonator with a directional coupler (DC): (a) schematic of the DC-coupled resonator and (b) expanded view of the coupler, showing the notation used in the text for the fields ($a$, $b$, $a'$, and $b$), the self-coupling coefficients $t_c$ and $t_c'$, the cross-coupling coefficients $\kappa_c$ and $\kappa_c'$, and the transmission $t_r'$ around the ring.

The next step in the derivation is to eliminate the factor $t_c t_c' - \kappa_c \kappa_c'$ in Eq. (4). In most previous derivations, it was assumed that the coupler is lossless [4], [5], but this is not a necessary assumption [12] and will not be made here. Since energy is conserved, the following Eq. (5) holds, as discussed, for example, in Ref. [13]:

$$|b|^2 + |b'|^2 = \alpha_c^2 |a|^2 + \alpha_c'^2 |a'|^2. \tag{5}$$

For generality, two separate loss functions $\alpha_c$ and $\alpha_c'$ for the coupler have been introduced, although usually by symmetry these two functions are equal. Scattering into radiation modes and absorption can contribute to $\alpha_c$ or $\alpha_c'$. Note it has been assumed that reflections are negligible.

Substituting $b$ and $b'$ from Eq. (1) and Eq. (2) into Eq. (5) gives the following relations, Eqs. (6), (7), and (8):

$$|t_c|^2 + |\kappa_c|^2 = \alpha_c^2; \tag{6}$$
$$|t_c'|^2 + |\kappa_c'|^2 = \alpha_c'^2; \tag{7}$$
$$t_c^* \kappa_c' + \kappa_c^* t_c' = 0. \tag{8}$$

Equations (7) and (8) lead to the following relation Eq. (9), which can be used in Eq. (4):

$$t_c t_c' - \kappa_c \kappa_c' = (t_c' t_c'^* + \kappa_c' \kappa_c'^*) \frac{t_c}{t_c'^*} = \alpha_c'^2 \frac{t_c}{t_c'^*}. \tag{9}$$

To simplify the final result, we introduce the phases $\phi_r'$ and $\phi_c'$ through Eqs. (10) and (11):

$$t_r' = |t_r'| e^{i\phi_r'}; \tag{10}$$
$$t_c' = |t_c'| e^{i\phi_c'}, \tag{11}$$

#115559 - $15.00 USD Received 10 Aug 2009; revised 21 Sep 2009; accepted 27 Sep 2009; published 6 Oct 2009

and define the following coefficients in Eqs. (12), (13), (14), and (15):

$$t \equiv |t_c'|/\alpha_c'; \tag{12}$$
$$\kappa \equiv |\kappa_c'|/\alpha_c'; \tag{13}$$
$$\alpha \equiv |t_r'|\alpha_c'; \tag{14}$$
$$\phi \equiv \phi_c' + \phi_r'. \tag{15}$$

Then Eq. (4) can be rewritten as Eq. (16):

$$\frac{b}{a} = \left(\frac{t - \alpha e^{i\phi}}{1 - \alpha t e^{i\phi}}\right) \frac{t_c}{t_c'^*} \alpha_c' e^{-i\phi_c'}. \tag{16}$$

Taking the absolute square of Eq. (16) gives Eq. (17):

$$T \equiv \left|\frac{b}{a}\right|^2 = \left|\frac{t_c}{t_c'^*}\right|^2 \alpha_c'^{\,2} \left(\frac{t^2 + \alpha^2 - 2\alpha t\cos\phi}{1 + \alpha^2 t^2 - 2\alpha t\cos\phi}\right) = \left|\frac{t_c}{t_c'^*}\right|^2 \alpha_c'^{\,2}\,\mathscr{T}, \tag{17}$$

where the factor $\mathscr{T}$ is defined as Eq. (18):

$$\mathscr{T} \equiv \left(\frac{t^2 + \alpha^2 - 2\alpha t\cos\phi}{1 + \alpha^2 t^2 - 2\alpha t\cos\phi}\right). \tag{18}$$

The quantities $t^2$ and $\kappa^2$ are the power splitting ratios of the coupler, and from Eq. (8) satisfy $t^2 + \kappa^2 = 1$. The quantity $\alpha^2$ is the power loss factor, and includes both propagation loss in the ring and loss in the coupler [14]. The factor $\mathscr{T}$ determines the shape of the resonances [9]; the other factors in Eq. (17) vary more slowly with wavelength,

Because $|\alpha_c|^2$ and $|t_r'|^2$ appear in $\mathscr{T}$ only through the product $\alpha^2$, the individual contributions $|\alpha_c|^2$ and $|t_r'|^2$ cannot be extracted from the shape of the resonances alone. In cases where the loss does not depend on $\lambda$, $\alpha_c$ and $t_r$ can be separated in principle by measuring $T$ at special wavelengths [10]. Alternatively, if all losses in the rest of the optical circuit could be accounted for, then the absolute value of $T$ could be measured and $\alpha_c$ could be determined from Eq. (17) once $\alpha$ and $t$ are known. We will not pursue either of these approaches here, and so only determine the total loss coefficient $\alpha$.

As a function of wavelength, $\mathscr{T}$ has a series of resonances; the transmission drops at those wavelengths where field amplitude builds up in the ring. The coefficients $\alpha$ and $t$ can be related to the width and depth of the resonances [7]. Let $\Delta\lambda_{\mathrm{FWHM}}$ be the full width at half maximum of a given resonance, and $\Delta\lambda_{\mathrm{FSR}}$ be the free spectral range (the wavelength separation between that peak and the adjacent peaks). The finesse $\mathscr{F}$ is defined by Eq. (19)

$$\mathscr{F} \equiv \Delta\lambda_{\mathrm{FSR}}/\Delta\lambda_{\mathrm{FWHM}}, \tag{19}$$

and the extinction ratio is defined by Eq. (20)

$$\mathscr{E} \equiv T_{\max}/T_{\min}. \tag{20}$$

Then the following relations Eqs. (21) and (22) follow from Eq. (18) for $\mathscr{T}$:

$$\mathscr{E} = \left[\frac{(\alpha + t)}{(\alpha - t)}\frac{(1 - \alpha t)}{(1 + \alpha t)}\right]^2; \tag{21}$$
$$\cos(\pi/\mathscr{F}) = \frac{2\alpha t}{1 + \alpha^2 t^2}. \tag{22}$$

#115559 - $15.00 USD Received 10 Aug 2009; revised 21 Sep 2009; accepted 27 Sep 2009; published 6 Oct 2009

These expressions reflect well-known properties of a ring resonator [4], [5]: if $\alpha = t$, then $T_{\min} = 0$ and $\mathscr{E}$ goes to infinity; if $\alpha t = 1$ (which requires both $\alpha = 1$ and $t = 1$), then $T_{\max} = T_{\min}$ and $\mathscr{F}$ goes to infinity.

Equation 22 can be solved for the product $\alpha t$, and that result can be substituted into Eq. (21). The result is a quadratic equation that yields $\alpha$ and $t$ as the two roots. The result can be written in terms of the following two quantities $A$ and $B$, defined by Eqs. (23) and (24):

$$A \equiv \frac{\cos(\pi/\mathscr{F})}{1+\sin(\pi/\mathscr{F})}; \tag{23}$$

$$B \equiv 1-\left[\frac{1-\cos(\pi/\mathscr{F})}{1+cos(\pi/\mathscr{F})}\right]\frac{1}{\mathscr{E}}. \tag{24}$$

In terms of these, $\alpha$ and $t$ are given by Eq. (25):

$$(\alpha,t) = \left(\frac{A}{B}\right)^{1/2} \pm \left(\frac{A}{B}-A\right)^{1/2}. \tag{25}$$

Because $\alpha$ and $t$ can be interchanged in $\mathscr{T}$ in Eq. (18), they appear as the two roots of a quadratic equation with no indication of which root corresponds to which quantity. Additional information is needed to identify them. As will be shown in Section 4, if the resonances are measured over a wide enough range of wavelength, $\alpha$ and $t$ may be distinguishable by their dependence on wavelength. For a directional coupler of physical length $L_c$ and a coupling length $L_\pi$ (the distance over which light is transferred from one arm of the coupler to the other), $t$ is given by Eq. (26) [10]:

$$t = \left|\cos\left(\frac{\pi L_c}{2L_\pi}\right)\right|. \tag{26}$$

For directional couplers $L_\pi$ decreases with $\lambda$ [10]; in the wavelengths and devices studied here, $1/L_\pi$ can be expanded reasonably accurately to first order in $\lambda$, leading to Eq. (27):

$$t \simeq \left|\cos(a_0 + a_1\lambda)\right|, \tag{27}$$

where $a_0$ and $a_1$ are constants. When the cross-coupling is strong, the characteristic sinusoidal variation is clear enough to distinguish $t$ from $\alpha$, as shown below.

Alternatively, $t$ and $\alpha$ could be distinguished by their dependence on device geometry, if different geometries are available. For example, keeping the same coupler geometry but increasing the radius of the ring will leave $t$ unchanged (to within tolerances in the fabrication) but will change $\alpha$. For small rings, when bending losses dominate, $\alpha$ will decrease as the ring is made smaller. For large rings, where propagation losses dominate, $\alpha$ will decrease as the ring is made larger.

Silicon photonic wires are known to be highly dispersive, as confirmed from the increase of $\Delta\lambda_{\mathrm{FSR}}$ with wavelength in our devices. The effects of dispersion are included in the above analysis, because $\Delta\lambda_{\mathrm{FSR}}$ and $\Delta\lambda_{\mathrm{FWHM}}$ are both related to the group index [10]. In principle, both $\mathscr{F}$ and $\mathscr{E}$ are only related to quantities $\alpha$ and $t$ for individual resonances, as shown in Eqs. (21) and (22). In practice, when values of $\Delta\lambda_{\mathrm{FSR}}$ are obtained from the separation between adjacent resonances, the dispersion is inevitably averaged over a non-zero range in wavelength, particularly for resonators with large $\Delta\lambda_{\mathrm{FSR}}$. In the devices studied here, however, this averaging introduces only small errors. For the smallest resonators (radius 5 $\mu$m), the FSR ($\sim$ 15 nm) changes only by about 3% between two adjacent resonance peaks.

#115559 - $15.00 USD Received 10 Aug 2009; revised 21 Sep 2009; accepted 27 Sep 2009; published 6 Oct 2009

## 3. Device fabrication and measurement

Ring resonators with directional couplers were fabricated as described in Ref. [3]. Devices were fabricated on Unibond SOI wafers with 2 $\mu$m thick buried oxide and 0.26 $\mu$m thick silicon core, with waveguides nominally 0.45 $\mu$m wide. Results from a selection of these resonators are shown below. The nominal gap in the DC section was 0.2 $\mu$m to 0.5 $\mu$m, and the length of the coupling section was 1 $\mu$m to 10 $\mu$m. All the devices discussed here had a single coupler and one input/output waveguide. (The analysis can be applied to add-drop devices, but this is not reported here.) The devices were fabricated as part of a study of biosensors, and many have long path lengths in a small footprint; results for folded or "hairpin" resonators are discussed below. The devices were covered with SU8 photoresist unless noted otherwise. Inverse tapers down to 150 nm in width were used at both the input and output facets to improve the coupling efficiency. These tapers also reduce the Fabry-Perot oscillations; without them, the oscillations can produce additional noise in the extracted values of $\alpha$ and $t$.

The devices were tested using a tunable laser coupled to the input facet via a polarization maintaining tapered fiber. An objective of 10 times magnification was used on the output side to collect the transmitted signal. The laser output was set to 1 mW, and the system has a setup loss of approximately $-5$ dB, which was not subtracted in the spectra shown below. The laser wavelength was scanned in steps of 1.5 pm to 20 pm. (The largest step was acceptable for broader resonances, but not for all devices.)

For each resonance in the measured spectrum, four quantities were determined: $T_{\max}$, $T_{\min}$, $\Delta\lambda_{\mathrm{FWHM}}$, and the wavelength of the minimum transmission. The value of $\Delta\lambda_{FSR}$ was found from the spacing between peaks or by assigning a peak index $m$ to each peak and fitting $\lambda(m)$ to a polynomial in $m$. Then $\alpha$ and $t$ were derived for each peak using Eq. (25).

## 4. Results and analysis

This section gives some examples of how $\alpha$ and $t$ determined from Eq. (25) can be disentangled. We start with a case where the strong variation of $t$ with $\lambda$ in the directional coupler makes it easy to distinguish $t$ and $\alpha$. Two devices are shown, with different path lengths of the ring. Then a device with even stronger cross-coupling is shown to illustrate further the sinusoidal variation of $t$ with $\lambda$. Finally, devices with weaker cross-coupling are compared, to show how different path lengths and coupler lengths can be used to separate $t$ and $\alpha$.

### *4.1. Coupler separation 0.3 $\mu$m*

Figure 2 shows the transmission of a folded or "hairpin" resonator. The device, shown in the insert, has a path length of 367.1 $\mu$m; the straight section of the coupler is 5 $\mu$m long and the two waveguides in the coupler are separated by 0.3 $\mu$m edge-to-edge. As shown in the inserts in the figure, $\Delta\lambda_{\mathrm{FWHM}}$ is smaller at the lower wavelengths than at the higher wavelengths.

Figure 3 shows $1/\mathscr{E} = T_{\min}/T_{\max}$ and $1/\mathscr{F} = \Delta\lambda_{\mathrm{FWHM}}/\Delta\lambda_{\mathrm{FSR}}$ determined from Fig. 2, and Fig. 4 shows the quantities $\alpha$ and $t$ calculated from $\mathscr{E}$ and $\mathscr{F}$. As discussed above, which curve is $\alpha$ and which is $t$ in Fig. 4 is not determined from the calculation, but the points obviously separate into two smoothly varying curves corresponding to the two quantities. In this case, one quantity is roughly independent of $\lambda$, and the other is decreasing with $\lambda$. The loss function $\alpha$ is expected to be a weak function of $\lambda$ in this device. Therefore the designation of $\alpha$ and $t$ in Fig. 4 was chosen so $\alpha$ corresponds to the curve that is almost independent of $\lambda$. On the other hand, $t$ can vary with $\lambda$ through Eq. (27); the solid line corresponds to a fit to $t$ from this equation. The values of $t$ are consistent with the dimensions of the coupler, as discussed in Ref. [10].

To confirm the assignments in Fig. 4, we consider a device with the same coupler and a longer path, where $\alpha$ should be smaller and $t$ similar to Fig. 4. Figure 5 shows the resonance

#115559 - $15.00 USD Received 10 Aug 2009; revised 21 Sep 2009; accepted 27 Sep 2009; published 6 Oct 2009

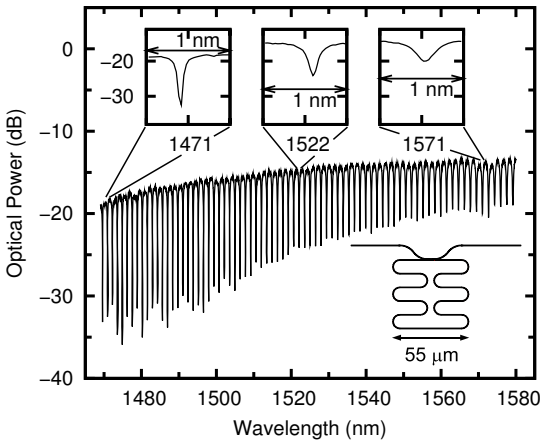


Fig. 2. Resonance spectrum for a folded resonator (shown schematically in the insert at the lower right) with cavity length 367.08 $\mu$m, coupler length 5 $\mu$m, and nominal separation 0.3 $\mu$m of the waveguides in the coupler. The minimum radius of curvature is 5 $\mu$m. The upper inserts show three expanded views over a 1-nm range centered at 1471 nm, 1522 nm, and 1571 nm.

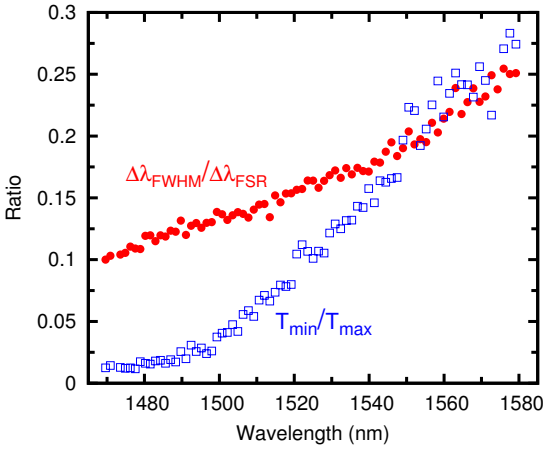


Fig. 3. Inverse of the extinction ratio $\mathscr{E} = T_{\max}/T_{\min}$ (open squares) and inverse of the finesse $\mathscr{F} = \Delta\lambda_{\rm FSR}/\Delta\lambda_{\rm FWHM}$ (closed circles), for the spectrum shown in Fig. 2.

#115559 - $15.00 USD Received 10 Aug 2009; revised 21 Sep 2009; accepted 27 Sep 2009; published 6 Oct 2009

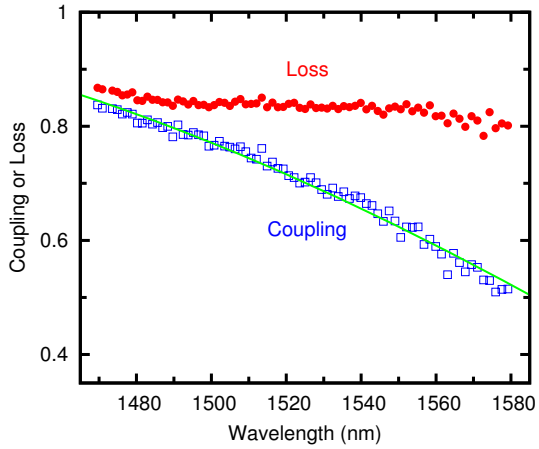


Fig. 4. Self-coupling coefficient $t$ (open squares) and loss coefficient $\alpha$ (closed circles) for the resonator spectrum in Fig. 2. The solid line through the squares shows a fit to Eq. (27), with $a_0 = -5.52$ and $a_1 = 4.14\ \mu\text{m}^{-1}$.

spectrum for such a device, from the same fabrication run, and Fig. 6 shows the corresponding $t$ and $\alpha$. Again, the branches were assigned so that the quantity varying most with $\lambda$ is assigned to $t$. The curves for $t$ in Fig. 4 and Fig. 6 are similar, supporting the assignment of those curves to $t$. At the wavelength where $\alpha$ and $t$ cross in Fig. 6, the resonances in Fig. 5 are deepest, corresponding to critical coupling where $\alpha \simeq t$ and $\mathscr{E} \simeq -25$ dB.

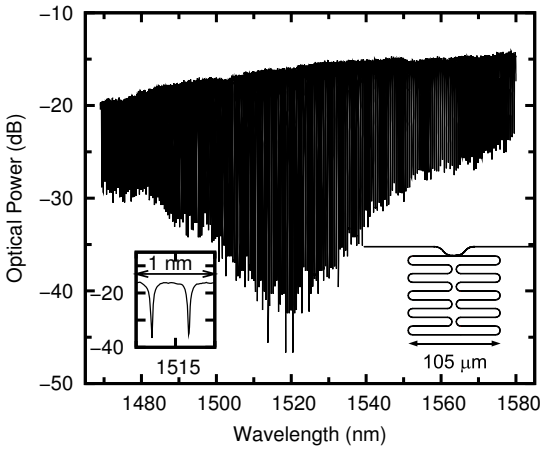


Fig. 5. Resonance spectrum for a folded resonator (shown schematically in the insert on the lower right) with cavity length 1112.7 $\mu$m, and the same coupler dimensions and minimum radius of curvature as the resonator in Fig. 2. The insert on the lower left shows an expanded view in a 1-nm range about 1515 nm.

#115559 - $15.00 USD Received 10 Aug 2009; revised 21 Sep 2009; accepted 27 Sep 2009; published 6 Oct 2009

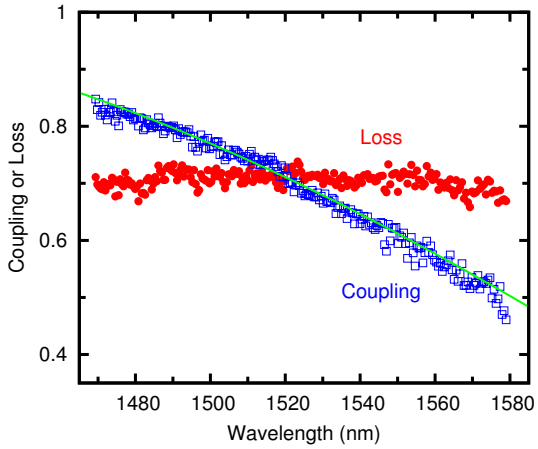


Fig. 6. Self-coupling coefficient $t$ (open squares) and loss coefficient $\alpha$ (closed circles) for the resonator spectrum in Fig. 5. The solid line through the squares shows a fit to Eq. (27), with $a_0 = -5.90$ and $a_1 = 4.40\ \mu\text{m}^{-1}$.

### 4.2. *Coupler separation 0.2 $\mu$m*

Figure 7 shows the resonance spectrum for a device with a longer DC coupler (10 $\mu$m) and a smaller separation (0.2 $\mu$m) than in the earlier examples. The spectrum has deep resonances near 1520 nm, and no resonances near 1560 nm. Figure 8 shows $t$ and $\alpha$ from this device. Again, the branches were assigned so that $\alpha$ is roughly independent of wavelength. This devices shows both critical coupling (near 1520 nm), as well as a region where $t$ approaches unity (near 1560 nm), where the resonances disappear. Since the depth of the resonances is less than the noise level in Fig. 7 near 1560 nm, no values can be extracted for $\mathscr{E}$ and $\mathscr{F}$, and consequently the coefficients in Fig. 8 show a gap in the wavelength range 1560 nm to 1570 nm, where $t \simeq 1$. This device serves as a good example to illustrate the method, but for many applications the coupling is unnecessarily strong. A similar device was analyzed in more detail in Ref. [10].

As discussed in Ref. [10], $L_\pi$ decreases with $\lambda$. For shorter couplers (as in the devices in Fig. 4 or Fig. 6), the argument of the cosine in Eq. (16) for $t$ is less than $\pi/2$, and $t$ therefore decreases with $\lambda$. In the device in Fig. 8, however, the longer $L_c$ and the smaller separation produces $L_c > L_\pi$, so that $t$ increases with $\lambda$, passes through a maximum (at $L_c = 2L_\pi$), and decreases again.

The coefficients $\alpha$ and $t$ in Fig. 8 appear to be discontinuous near 1520 nm. This is a consequence of the "anticrossing" of the two roots of Eq. (25). The difference between the two roots is, from Eq. (15), given by Eq. (28):

$$|\alpha - t| = 2\sqrt{\frac{A}{B}}\sqrt{1-B} \propto \frac{1}{\sqrt{\mathscr{E}}}, \tag{28}$$

where the proportionality follows from the definition of $B$ in Eq. (14). If stray light enters the detector and prevents $\mathscr{E}$ from rising above some limiting value $\mathscr{E}_0$, then the two roots will not be equal at critical coupling, but rather will differ by an amount proportional to $1/\sqrt{\mathscr{E}_0}$. Thus when the assignment of $t$ and $\alpha$ is switched between the two branches, there is an apparent discontinuity in the two quantities. It would be straightforward to correct for this by determining the intensity of the stray light and subtracting it from the measured intensity.

#115559 - $15.00 USD Received 10 Aug 2009; revised 21 Sep 2009; accepted 27 Sep 2009; published 6 Oct 2009

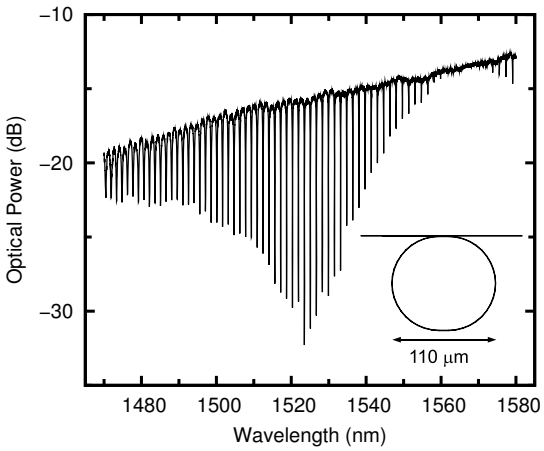


Fig. 7. Resonance spectrum for a resonator with racetrack geometry (shown schematically in the insert) with radius 50 $\mu$m, cavity length 334.16 $\mu$m, coupler length 10 $\mu$m, and nominal separation 0.2 $\mu$m of the waveguides in the coupler.

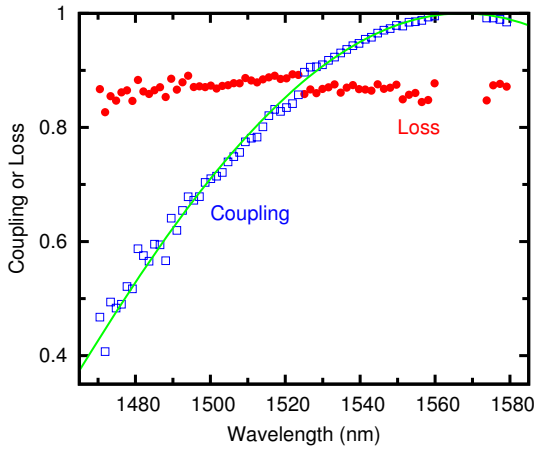


Fig. 8. Self-coupling coefficient $t$ (open squares) and loss coefficient $\alpha$ (closed circles) for the resonator spectrum in Fig. 7. The solid line through the squares shows a fit to Eq. (27), with $a_0 = -15.05$ and $a_1 = 11.61\ \mu\text{m}^{-1}$.

#115559 - $15.00 USD Received 10 Aug 2009; revised 21 Sep 2009; accepted 27 Sep 2009; published 6 Oct 2009

### *4.3. Coupler separation 0.4 $\mu$m and 0.5 $\mu$m*

If the resonators have low loss and the cross-coupling is weaker than in the previous examples, both $t$ and $\alpha$ may be near unity. Then it is more difficult to separate $t$ and $\alpha$ based on the wavelength dependence alone. Instead, a series of devices of different dimensions or different coupling geometry can be used.

As an example, Fig. 9 shows six resonators with racetrack geometry, similar to that shown in the insert to Fig. 7. Three design parameters, namely radius $R$, coupler length $L_c$, and coupler spacing $S_c$, are noted in each panel in the figure as $(R, L_c, S_c)$, all in micrometers. The four devices in the left and middle panels all have $R = 5$ $\mu$m, and $L_c$ and $S_c$ take on the four possible combinations of $L_c = 1$ $\mu$m or $L_c = 5$ $\mu$m and $S_c = 0.4$ $\mu$m or $S_c = 0.5$ $\mu$m. These four devices should therefore have similar $\alpha$, and different $t$. The devices in the right-most panels have a smaller $R = 2$ $\mu$m, and the same values of $L_c$ and $S_c$ as the devices in the middle panels. For these two smaller devices, $t$ should be similar to that for the devices in the middle panels. On the other hand, $\alpha$ of these smaller devices could be either larger than $\alpha$ of the other four devices if bending loss dominates, or smaller if propagation loss dominates.

Figure 9b shows $\alpha$ and $t$ extracted from the spectra, and assigned to give a consistent picture for all six devices. The losses are similar in all four left and center panels. The coupling in those panels varies consistently with the values of $S_c$ and $L_c$. For $S_c = 0.5$ $\mu$m and $L_c = 1$ $\mu$m, $t$ is largest and varies the least with $\lambda$. Conversely, for $S_c = 0.4$ $\mu$m and $L_c = 5$ $\mu$m, $t$ is smallest and varies most with $\lambda$ of the four devices. (Note the assignment of $\alpha$ and $t$ for the upper left device is arbitrary because the two quantities are so similar at each $\lambda$.)

Once these assignments are made, $t$ in the smaller devices (right panels) can be identified by comparing with the middle panels, leaving $\alpha$ as the other curve. The losses are higher in the smaller device, not smaller, implying that bending losses are the dominant losses in devices with $R = 2$ $\mu$m. This is consistent with numerical calculations [15].

## 5. Conclusions

We have developed a simple method to extract the loss and self-coupling coefficients of simple (all-pass) ring resonators, using the spectral dependence of the transmission of a single resonator (or a comparison of a few resonators with different design parameters). Although the self-coupling and loss coefficients at a given wavelength can be extracted from the shape and spacing of the resonance at that wavelength, the analysis does not distinguish coupling from loss. It is possible to disentangle the two quantities with more complicated structures, but such devices might not be available. We have shown how the two coefficients can be disentangled based on their behavior with wavelength, with further information if necessary from variations in the device geometry. Although this can require devices with different coupler geometry or path length, such variations in design are often available as part of a search for the optimum parameters for the application one has in mind.

#115559 - $15.00 USD Received 10 Aug 2009; revised 21 Sep 2009; accepted 27 Sep 2009; published 6 Oct 2009

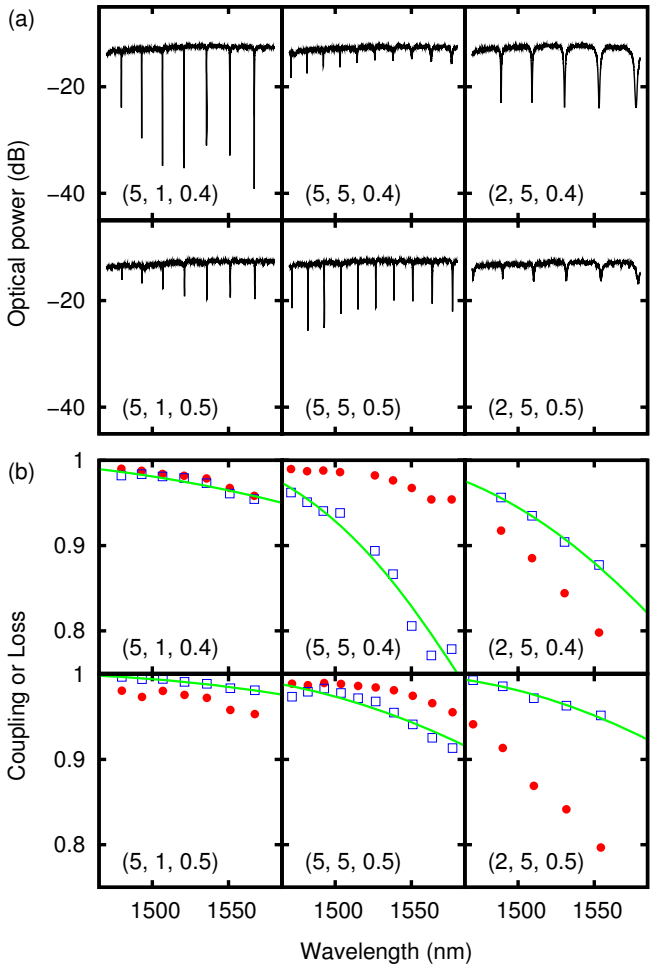


Fig. 9. (a) Resonance spectrum for six racetrack resonators. The three values in parentheses in each panel give the values of radius $R$, coupler length $L_c$, and separation $S_c$ between the waveguides, all in micrometers. These devices were not covered with SU-8 photoresist. (b) Self-coupling coefficient $t$ (open squares) and loss coefficient $\alpha$ (closed circles) for the resonator spectra in Fig. 9. The solid line through the squares shows fits to the expression in Eq. (27). From left to right, then top to bottom, the values of $a_0$ are $-1.96$, $-6.03$, $-4.49$, $-1.86$, $-2.99$, and $-3.31$; the values of $a_1$ are 1.44, 4.27, 3.22, 1.31, 2.15, and 2.33 $\mu$m$^{-1}$.

#115559 - $15.00 USD Received 10 Aug 2009; revised 21 Sep 2009; accepted 27 Sep 2009; published 6 Oct 2009